Chitosan as a paradigm for biopolymer electrolytes in solid-state dye-sensitised solar cells

Chitosan as a paradigm for biopolymer electrolytes in solid-state dye-sensitised solar cells

Noriah Abdul Rahman,[1] Sharina Abu Hanifah,[1,2] Nadhratun Naiim Mobarak,[1,2] Azizan Ahmad,[1,2,3] Norasikin Ahmad Ludin,[4] Federico Bella[5,*] and Mohd Sukor Su'ait[4,*]

[1] Faculty of Science and Technology, Universiti Kebangsaan Malaysia, 43600, Bangi, Selangor Darul Ehsan, Malaysia

[2] Polymer Research Center (PORCE), Faculty of Science and Technology, Universiti Kebangsaan Malaysia, 43600, Bangi, Selangor Darul Ehsan, Malaysia

[3] Research Center for Quantum Engineering Design, Faculty of Science and Technology, Universitas Airlangga, 60115, Surabaya, Indonesia

[4] Solar Energy Research Institute (SERI), Universiti Kebangsaan Malaysia, 43600, Bangi, Selangor Darul Ehsan, Malaysia

[5] Electrochemistry Group, Department of Applied Science and Technology, Politecnico di Torino, 10129, Turin, Italy

Corresponding authors: mohdsukor@ukm.edu.my; federico.bella@polito.it

Keywords: biopolymer electrolyte; chitosan; dye-sensitized solar cell; solid-state electrolyte; biosourced polymer; solid-state photovoltaics.

Abstract

Biopolymers are among the most promising electrolyte hosts for different electrochemical devices in the energy conversion and storage fields. In this work, the potential of chitosan as biopolymer laden with NaI salt is explored and applied as solid polymer electrolyte for dye sensitised solar cells. The chitosan-NaI electrolyte is successfully prepared via a simple and upscalable solution casting technique. Infrared spectroscopy analysis highlights interactions between chitosan and NaI, that weaken the semi-crystalline domains of chitosan and favour the conduction of the redox shuttle ions between cell electrodes. At room temperature, the best ionic conductivity was obtained for the

samples laden with NaI 30 wt%, with values equal to 1.11×10^{-4} S cm^{-1}. Na^+ transference number determination indicates that only 0.9% of the ionic conductivity is determined by these cations, thus highlighting that I^- anions represent the active species in the newly proposed solid-state electrolyte. This result is highly desired considering that these anions are those responsible for the regeneration of oxidized dye molecules in the cell and, overall, for the cell efficiency. Current-voltage measurement of solid-state photovoltaic devices under simulated sunlight led to a reproducible and stable power conversion efficiency of 0.06%, along with a short-circuit current density of 0.32 mA cm^{-2}, an open circuit voltage of 0.7 V and a fill factor 0.3.

1. Introduction

Solar cells are getting every day more attention due to issues like the pollution and shortage of energy sources from carbon-based fuels [1,2]. Solar energy can be the promising future energy source since it is abundant, clean, safe and silent [3,4,5,6]. Dye-sensitised solar cells (DSSCs), famously known as Grätzel cells, are categorised as an emerging generation of solar cell possessing low manufacturing cost, high conversion efficiency and simple preparation technique [7,[8]]. Most of the DSSCs with high efficiency up to ≈14% use liquid electrolytes (LEs), typically based on organic solvents solubilizing a redox shuttle [9,10]. Although these LEs lead to high efficiency values, they cause relevant issues such as leakage, difficulties in sealing and fabrication processes, safety problems and corrosion of metal components, leading to an overall poor long-term stability [11]. Therefore, solid polymer electrolytes (SPEs) represent a strong solution to this issue and are now considered as a Holy Grail in the field of DSSCs, since they would be able to freeze the degradation of cell performance upon time [12,13].

SPEs consisting of complexes of alkali metal ions within a polymeric matrix were proposed by Fenton and Wright [14]. They used sodium- and potassium-based salts and poly(ethylene oxide) (PEO) for the preparation of the first polymer electrolytes. The research on SPEs has continued

and today is a cutting edge topic in the field of solid-state electrochemistry [15,16]. SPEs are able to form good interfaces with electrodes surfaces and they are leakage-free, easy to seal and typically show wide electrochemical stability windows [17]. Additionally, SPEs possess desirable properties such as easy assembly of films in various shapes, sizes and designs, which are suitable for various electrochemical devices assembly, including batteries [18], fuel cells [19], supercapacitors [20] and solar cells [21,22,23]. All of these advantages make SPEs as a promising replacement for LEs in DSSCs.

According to Park *et al.* [24], the polymeric matrix for a good SPE needs to possess some characteristic to target high ionic conductivity values. The polymeric matrix requires the presence of polar groups, mainly containing oxygen (O), nitrogen (N) and sulphur (S). These polar groups can give to the material a dipole moment that affects the dielectric polarisation. Thus, intermolecular interactions between these functional group and alkali metal ions are created, leading to the solvation of salt and mimicking a solid-state version of a liquid electrolyte system.

To avoid the use of synthetic polymers, which are not biodegradable and derive for production processes that could not be seen as compatible with the sustainable requirements of DSSCs, the researchers started to explore materials from the agriculture industry when producing novel polymer electrolytes, such as cellulose [25], agar [26,27], starch [28], alginate [29], carrageenan [30] and chitosan [31].The use of these biopolymeric materials contributes to minimizing environmental issues, as well as lowering the cost of solar cells [32].

Chitosan is also known as a chitin derivative when it is dissolved in diluted acid, *e.g.* acetic acid [33].It is composed of two main groups, *i.e.* glucosamine and *N*-acetyl glucosamine units, which are linked by β-1,4-glycosidic bonds. Chitosan possesses polar functional groups such as hydroxyl and amine, which are important in salt complexation and solvation [22]. Chitosan has previously been doped with ammonium salt, like NH_4NO_3 [34,35,36], $NH_4CF_3SO_3$ [31,37], NH_4F [37,38], NH_4Br [39],NH_4I [40],NH_4SCN [41,42], CH_3COONH_4, NH_4Cl and $(NH_4)_2SO_4$ [43]. It has also

been doped with several lithium salt, like $LiCF_3SO_3$ [44,45], lithium acetate (LiOAc) [46,47], $LiNO_3$ [48], LiTFSI [49], $LiClO_4$ [50], as well as sodium salts, such as NaI [51] and $NaCF_3SO_3$ [52]. Therefore, chitosan could represent an intriguing polymeric matrix for the preparation of solid-state electrolytes for DSSCs.

Some applications of chitosan-based biopolymer electrolytes in DSSCs were published in the previous years, mainly in two physical states, *i.e.* solid and quasi-solid. As regards solid-state, Buraidah *et al*. used chitosan as electrolyte matrix, but due to the low efficiency they added a plasticizer and a ionic liquid [53], while in another work they blended chitosan with other polymer, such as PEO [54]. Overall, this made poor the choice of a biopolymer electrolyte. Singh *et al*. doped a chitosan/salt system with a ionic liquid as well [55]. Instead, as regards gel-state systems, chitosan was mixed with nanoparticles, KI and NH_4I salts and organic solvents [56].In other studies, chitosan derivatives were prepared, namely *N*-phtaloyl chitosan and hexanoyl chitosan: the former was doped with single [57] and binary [58] salts, leading to gel-state systems; instead, hexanoyl chitosan was blended with polyvinyl chloride and a ionic liquid, 1-methyl-3-propylimidazolium iodide (MPImI) [59]. Again, trying to improve cell sustainability and choice of oil-free components is weakened if plasticizers and ionic liquids are added in the chitosan-based electrolyte.

In this work, NaI was chosen as a simple and cheap doping salt for a chitosan biopolymeric matrix, and the resulting true solid-state electrolyte was used to fabricate lab-scale DSSCs. The chemical interactions, structural and thermal properties, morphology and electrochemical characterizations were investigated. As a result, chitosan with NaI were demonstrated to contribute to high ionic conductivity in the solid-state form, due to the presence of two main polar functional groups (hydroxyl and amine) in the biopolymer structure, supporting proper cell operation upon time.

2. Material and methods

2.1 Chemicals

Chitosan, medium molecular weight (M_w = 190,000-310,000 g mol^{-1}) was commercially obtained from Sigma-Aldrich. NaI and glacial acetic acid were supplied by Systerm ChemAR.

2.2 Preparation of biopolymeric SPEs

Preparation of solid biopolymeric SPEs was carried out by solution casting technique. Chitosan (1 g) was dissolved in 1 wt% acetic acid aqueous solution (50 mL) into six different conical flasks. Then, varied amounts of NaI (5-30 wt%) were added into the chitosan solution. The mixtures were stirred continuously with a magnetic stirrer until the solution became homogeneous, and then they were poured into a petri dish. The solution was left to evaporate slowly to form films at ambient temperature. A free-standing, clear, homogenous film was obtained for all systems. The films were kept in desiccators before being characterised.

2.3 Impedance analysis

To determine the ionic conductivity of biopolymeric SPEs, the bulk resistivity (R_b) of film-shaped samples was obtained by electrochemical impedance spectroscopy (EIS), using a Hioki 3532-50 LCR Hi-Tester in the frequency range from 0.1 Hz to MHz and 100 mV amplitude. SPE films were previously cut into small discs of 2 cm diameter. Then, the films were placed in a sandwich architecture between the stainless-steel ion-blocking electrodes, with a surface contact area of 1.723 cm^2, and connected to the instrument. R_b was determined from the equivalent circuit analysis by using Z-sim software. The complex impedance data, Z^* were processed by Z-sim in a complex impedance plot (Cole-Cole plot), where the imaginary part, Z_i (Z') was plotted against its real part Z_r (Z'') by the relation:

$$Z^* = Z_r + j\,Z_i \qquad (1)$$

The temperature-dependent analysis was performed from the room temperature of 303 K until 393 K. The electrical conductivity (σ) of the films was calculated from the equation:

$$\sigma = \frac{t}{R_b \cdot A} \qquad (2)$$

where t is the film thickness and A is the electrode-electrolyte contact area. The mechanism of ionic conduction in the SPE system can be investigated throughout the temperature-dependent study. From the plot of $log\sigma$ *vs.* 1000/T, the activation energy can be calculated by the Vogel-Tamman-Fulcher (VTF) model:

$$\sigma = \sigma_0 \cdot e^{-\frac{B}{T-T_0}} \qquad (3)$$

where σ_0 is the conductivity at infinite temperature, the parameter B is the pseudo-activation energy for ionic conduction expressed in temperature units, T_0 is the corrected glass transition temperature (i.e., $T_0 = T_g - 50$).

Investigation on dielectric properties included the dielectric constant, the dielectric loss, the ions relaxation the and electrical modulus. The equations used to determine for the dielectric constant (ε_r), the dielectric loss (ε_i), the real electrical modulus (M_r) and the imaginary electrical modulus (M_i) are these:

$$\varepsilon_r = \frac{Z_i}{\omega \cdot C_0 \cdot (Z_r^2 + Z_i^2)} \qquad (4)$$

$$\varepsilon_i = \frac{Z_r}{\omega \cdot C_0 \cdot (Z_r^2 + Z_i^2)} \qquad (5)$$

$$M_r = \frac{\varepsilon_R}{(\varepsilon_r^2 + \varepsilon_i^2)} \qquad (6)$$

$$M_i = \frac{\varepsilon_i}{(\varepsilon_r^2 + \varepsilon_i^2)} \qquad (7)$$

where $C_0 = \frac{\varepsilon_0 \cdot A}{t}$ is the vacuum capacitance, ε_0 is the permittivity of the free space, $\omega = 2\pi \cdot f$ is the angular frequency and f is the frequency. The dielectric constant (ε_r), also known as relative permittivity when using the symbol ε_0^*, is expressed as [60]:

$$\varepsilon_r = \frac{\varepsilon}{\varepsilon_0} \qquad (8)$$

When the polarity of the electric field reverses rapidly, there will be some energy losses, called dielectric loss, as ions move and dipoles align. Both ε_r and ε_i are related to the electrical conductivity of the materials.

Another relevant parameter used in dielectric studies is $\tan \delta$. It is used to observe and analyse the relaxation behaviour in the polymer electrolyte, which can be calculated as:

$$\tan \delta = \frac{Z'}{Z''} \quad (9)$$

2.4 Infrared spectroscopy analysis

Infrared spectroscopy analysis was carried out using attenuated total reflection - Fourier transform infrared spectroscopy (ATR-FTIR), by a PerkinElmer Spectrum 400 FT-IR-NIR spectrophotometer. Transmittance spectra were collected in the range from 4000 to 650 cm^{-1}, with a resolution of 2 cm^{-1}. This analysis was conducted to observe the vibration modes within the biopolymeric SPEs.

2.5 Structural analysis

X-ray diffraction (XRD) was used to study the cristallinity of bipolymeric SPEs. XRD was carried out using a D8 Advance instrument by Bruker. The samples were cut into a suitable size and adhered onto a glass slide. Then, the glass slide was placed in the sample holder of the diffractometer. The samples were scanned from the range diffraction angle of 2° to 80°, with a scan rate of 0.05° s^{-1}. The analysis was done at room temperature.

2.6 Morphological analysis

Cross-sectional morphology of biopolymeric SPEs was observed using a Zeiss Merlin Compact scanning electron microscope (SEM) at ×500 and ×10,000 magnifications, with an accelerating voltage of 3.0 kV. The samples were prepared by breaking them into small rectangular shapes, following by a coating step with iridium under vacuum conditions.

2.7 Thermal analysis

Thermal properties of chitosan powder were determined by differential scanning calorimetry (DSC), with a Mettler Toledo instrument. T_g data reported in the manuscript were obtained from the second heating run, at a rate of 10 °C min^{-1}, from 25 to 200 °C under nitrogen atmosphere. Thermogravimetric analysis (TGA) was carried out to investigate the decomposition temperature of chitosan samples. The samples were heated from 25 to 600 °C under argon flow at a heating rate of 10 °C min^{-1}, using a Mettler Toledo instrument.

2.8 Chronoamperometry analysis

The ionic conduction in an electrolyte is proved by performing transference number study using Wagner's DC polarization method, from which ionic (t_{ion}) and electronic (t_{ele}) transport contributions can be determined. The DC current was monitored as a function of time by applying a constant DC voltage (0.01 V) across the sample mounted between two stainless steel electrodes [61]. t_{ion} and t_{ele} are given by these equations:

$$t_{ion} = \frac{I_i - I_s}{I_s} \qquad (10)$$

$$t_{ele} = 1 - t_{ion} \qquad (11)$$

where I_i and I_s are the total and residual currents, respectively.

Sodium ion transference number (t_{Na^+}) was determined using the DC polarization method. Current was monitored as a function of time as fixed DC voltage (0.01 V) applied across the sample sandwiched between symmetrical sodium metal electrodes (Na/sample/Na), externally faced to stainless steel plates. t_{Na^+} was calculated by this equation [62]:

$$t_{Na^+} = \frac{I_{SS}\cdot(\Delta V - I_0\cdot R_0)}{I_0\cdot(\Delta V - I_{SS}\cdot R_{SS})} \qquad (12)$$

where I_{SS} is the initial current at the steady state, I_0 is the initial total current, ΔV is the applied potential, R_0 is the initial resistance of the passivation layer and R_{SS} is the resistance of the passivation layer (steady state current).

2.9 Voltammetry analysis

Electrochemical stability of the electrolyte, electrode and metal can be evaluated by using linear sweep voltammetry (LSV) by adopting different types of electrodes and different configurations between electrodes and electrolyte. To determine the electrochemical stability of the electrolytes, stainless steel blocking electrodes were used, in the range from 0 to 6 V and at a scanning rate of 100 mV s^{-1} at room temperature, choosing the most conducting sample. The potential was applied to the working electrode and was varied linearly upon time.

2.10 DSSCs fabrication

Each DSSC was fabricated by following the standard procedure outlined by the Solaronix company. Photoanode glass was spread with TiO_2 paste using a spin coater with the support of an adhesive tape to prevent it from moving. Different TiO_2 layers were deposited by spin coating. Then, in order to reach the anatase phase, each electrode was annealed at 450 °C for 30 min. Subsequently, it was immersed in 0.3 mM of N719 dye solution at room temperature for 24 h. As regards the cathode, a platinised FTO counter electrode was prepared by the doctor blade technique and annealed at 450 °C for 30 min.

SPEs containing NaI were put together with I_2 (at a NaI:I_2 molar ratio of 10:1) in a closed glass container, where I_2 sublimated into the biopolymeric film. The reference liquid electrolyte was prepared with the same composition of NaI and I_2.

The assembly procedure of DSSCs is shown in **Figure 1**.

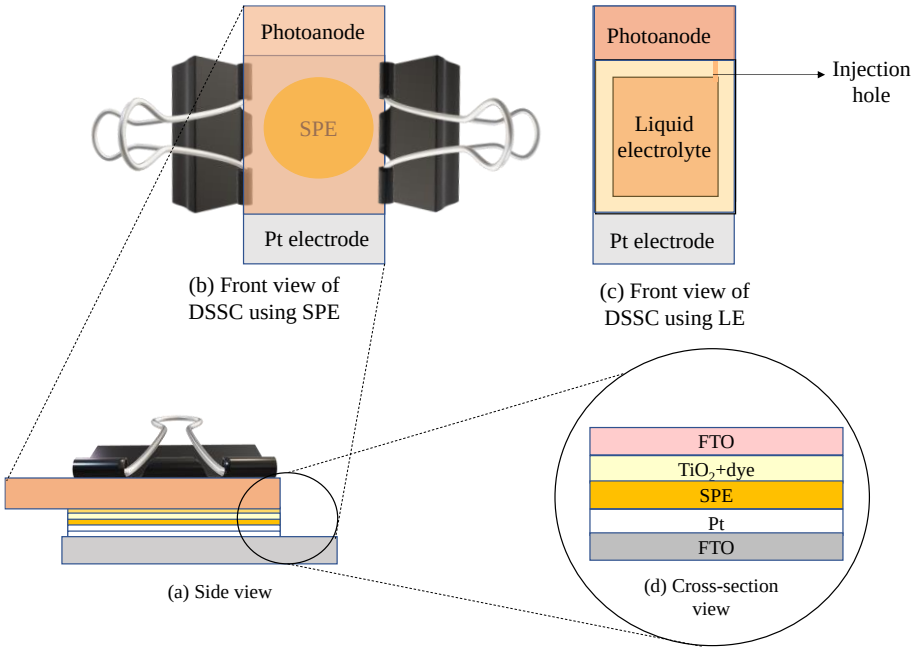

Figure 1. The assembly procedure of FTO/TiO_2-dye/SPE/Pt DSSCs from several viewpoints: (a) side view, (b) front view, using SPE, (c) front view, using LE, (d) cross-section view.

2.11 Photovoltaic characterization

The current-voltage (I–V) data of the fabricated DSSCs were recorded by Keithley 237 with a xenon light source, at room temperature (dark atmosphere) and under AM (air mass) 1.5 illumination, at a light intensity of 100 mW cm^{-2} controlled by a lux meter. The active area of cells was set to 0.1 cm^2. The photoelectric performances, such as the fill factor (FF) and light-to-electricity conversion efficiency (η) were calculated by these equations:

$$FF = \frac{V_{max} \cdot J_{max}}{V_{oc} \cdot J_{sc}} \qquad (13)$$

$$\eta = \frac{V_{oc} \cdot J_{sc} \cdot FF}{P_{in}} \qquad (14)$$

where V_{oc} is the open circuit voltage, J_{sc} is the short circuit current density, P_{in} is the incident light power density, V_{max} and J_{max} are the voltage and the current density values in the J–V curves, respectively, at the point of maximum power output [63].

The incident photon to current conversion efficiency (IPCE), also termed as external quantum efficiency of the solar cell, relates to the photocurrent density produced in the external circuit under

monochromatic illumination of the cell divided by the photon flux that strikes the cell. In other words, it is a measure of how efficient the device converts incident photons in electrons at precise wavelength values. IPCE can be calculated according to this equation:

$$IPCE = 1240 \cdot \frac{J_{ph}}{\lambda \cdot P_{in}} \qquad (15)$$

where J_{ph} is the short-circuit current density generated by the monochromatic light and λ is the wavelength. The IPCE can also be expressed by:

$$IPCE = LHE \cdot \phi_{inj} \cdot \phi_{reg} \cdot \eta_{cc} \qquad (16)$$

where LHE is the light harvesting efficiency, ϕ_{inj} is the quantum yields of electron injection, ϕ_{reg} is the dye regeneration and η_{cc} is the charge collection efficiency.

3. Results and discussion

3.1 EIS analysis

Impedance analysis is typically used to study the electrical properties of electrodes and polymer electrolytes. The logarithm of conductivity values measured at room temperature in function of the salt amount for biopolymeric SPEs is shown in **Figure 2(a)**. The plot shows that the conductivity of the electrolyte gradually increased when the NaI salt concentration raised, from 8.88×10^{-10} S cm^{-1} (NaI-free) to the optimum value of 1.11×10^{-4} S cm^{-1} (NaI 30 wt%). The plot gives information about the interaction between salt and chitosan matrix. Indeed, as NaI salt content increased, the number of mobile ions in the electrolyte became higher and, as a result, the ionic conductivity was improved. This enhancement of the ionic conductivity derived from the ions dissociation, bringing Na^+ and I^- free motion in the biopolymeric host matrix.

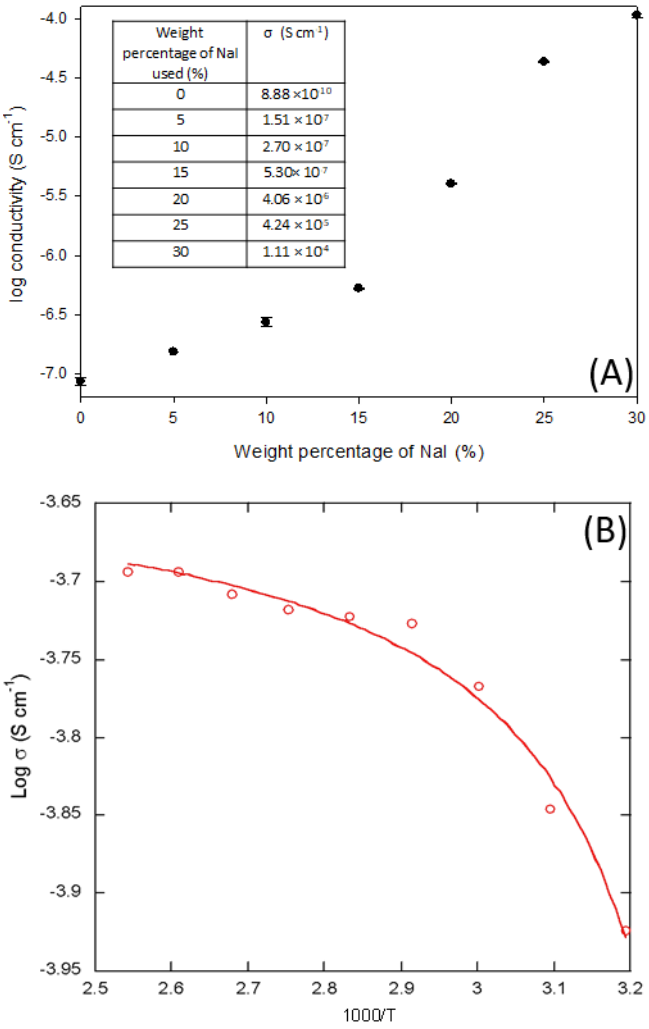

Figure 2. (a) Room temperature ionic conductivity of biopolymeric SPEs containing with different amuonts of NaI; **(b)** log σ *vs.* 1000/T plot for the SPE containing NaI 30 wt%.

The mechanism of ionic conduction in the biopolymeric SPE can be investigated through temperature-dependent studies. **Figure 2(b)** shows the temperature dependence of ionic conductivity for a sample laden with NaI 30 wt%, *i.e.* the best samples come out from room temperature analysis. Its ionic conductivity increases up to 7×10^{-4} S cm^{-1} at 393 K, thus showing that the ions experienced higher mobility as the temperature raised. The experimental data were fitted following the Arrhenius model; however, the regression coefficient was far from unity. Therefore, we tried to fit our data with the VTF equation and we got a regression coefficient of 0.99. VTF parameters extracted from the fitting were: i) $\sigma_0 = 2.33\times10^{-4}$ (±0.01) S cm^{-1}, which is

associated to the number of charge carriers in an electrolyte system; ii) $B = 5.549$ (±1) kJ mol^{-1} as pseudo-activation energy for ion transport; $T_0 = 21.29$ (±4) °C, which is usually 30 to 50 °C lower than the T_g obtained by DSC measurements [64].

The non-linearity of the conductivity with the temperature indicates that ions transport in biopolymeric SPEs is dependent on the macromolecular segmental motion, which results from the existence of a free volume. When the electrical field is applied, the ions will diffuse into the free volume [65]. When the temperature increases, the polymer chains easily move and facilitate ions transport.

Trends of ionic conductivity in the biopolymeric SPEs can be further studied by dielectric measurements, which can help to understand better the polarization effect at the electrode/electrolyte interface. The dielectric study also investigates the relationship between ionic relaxation time and conductivity. In particular, the dielectric constant can be considered as a measurement of the material polarization and it is related to the capability of a substance to store charges in the electric field. The plots showing ε *vs.* $\log f$ at room temperature for biopolymeric SPEs containing different NaI amount are given in **Figure 3**. The value of ε_r (see **Figure 3(a)**) increases as the frequency decreases, and this is particularly evident for the best conducting sample (i.e., the one based on NaI 30 wt%). As the amount of NaI increased from 5 to 30 wt%, the stored charge in the sample also increased, justifying the observed trend. The higher value of dielectric constant might be due to the dissociation of the salt in the biopolymeric matrix. A higher value of dielectric constant gives the ability to dissociate more salt into cations and anions, thus incrementing the density of mobile ions in the space charge accumulation region, hence bringing to a conductivity increase [39]. Conversely, the low value in dielectric constant limits the dissociation degree of the salt.

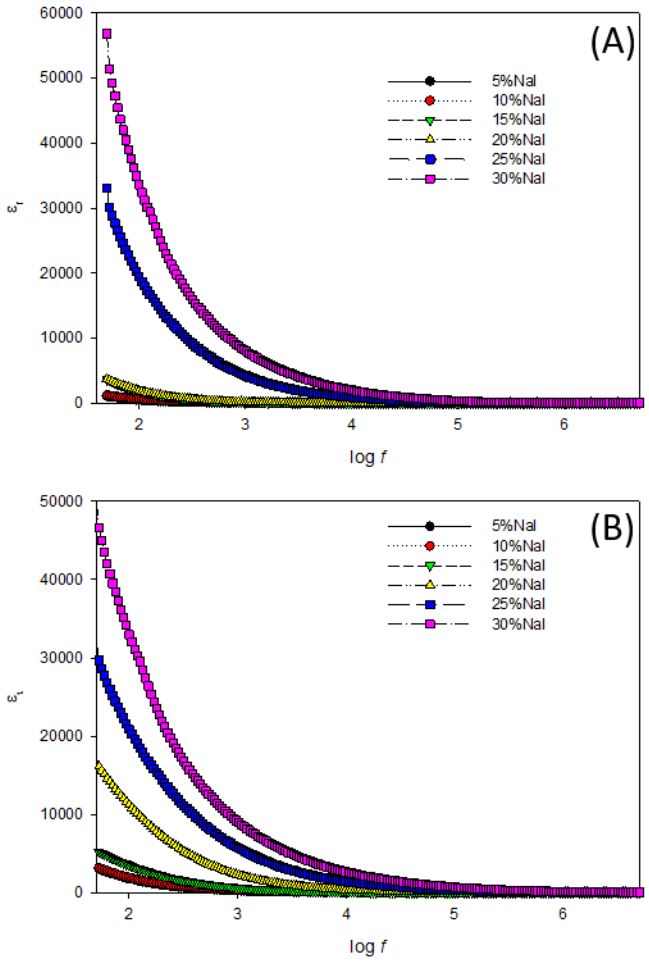

Figure 3. (a) Frequency-dependent real part and **(b)** imaginary part of dielectric constant *vs.* frequency for biopolymeric SPEs laden with different amounts of NaI at room temperature.

Under an electric field, ions in the electrolyte (Na^+, H^+, CH_3COO^-, I^-) will diffuse and migrate along the field at the blocking electrode. At low frequencies (1 to 3 Hz), as shown in **Figure 3**, ε_r rises due to the electrode polarization. Electrode polarization or interfacial polarization occurs when the ions are unable to cross the electrode/electrolyte interface, due to the usage of blocking electrode, so the ions will accumulate at the electrode/electrolyte interface until hetero-charge layers form. This situation is totally diverse at the high frequency region. At the high frequency region (4 to 6 Hz), there are no excess ions accumulating at the electrode/electrolyte interface, due to the periodic reversal of applied electric field occurring in a short period. The dielectric constant decreases rapidly until it becomes frequency-independent in this region. Besides that, the

accumulated ions at the interface become localized and this will reduce the influence of charge carriers towards the electrode. This phenomenon can be well enlightened by non-Debye type, which explains in detail the ions diffusion behaviour of the observed space charge region in the frequency format [66].

Dielectric loss (ε_i) *vs.* $\log f$ plot is presented in **Figure 3(b)**. ε_i values showed the same trend as that of ionic conductivity. Energy loss has been caused by heat through internal friction, generated during the polarization process. The value of dielectric loss is the reflection of the amount of energy dissipating and degree of out of phase in the electrical field, as can be seen in the imaginary part of the complex relative permittivity. Dielectric loss for the sample laden with NaI 30 wt% showed an optimal energy loss to move ions and align dipoles when the polarity of the electric field reversed rapidly; hence, this explained the optimal conductivity in the samples series.

Analysis on dielectric behaviour can be confirmed using dielectric moduli described by equations (6) and (7). This analysis gives emphasis on the bulk dielectric behaviour and highlights the effect of electrode polarization. **Figure 4** shows the variation of real and imaginary parts of the dielectric modulus. At low frequency values (1-4 Hz), the values of M_r and M_i approach zero, as it can be observed by the long tail. This long tail indicates a large capacitance associated to electrode polarization. The electrode polarization is negligible in this region. Definite peaks are not well observed in **Figure 4(b)** because the spectra shifted to the right part as the weight percentage of NaI increased, going beyond the frequency window of the experimental analysis. Thus, the plot only shows the dispersion part. At higher frequencies (4-7 Hz), the values of M_r and M_i increase, and this can be observed as a curved peak. Modulus value increases with frequency due to the bulk effect. According to Gunn *et al.* [67], who discovered the bulk effect, the electron transfer and avalanche transit time are the two elements regarding the bulk effect and, in this research, transferred electron caused the bulk effect [68]. M_r increases with frequency and reaches a maximum at higher frequencies; this may be attributed to a poor restoring force that controls the

mobility of ion by an induced electric field [69]. This suggests that the conduction mechanism is the result of the long-range mobility of charge carriers, which indicates that the biopolymeric SPEs are ionic conductors [70].

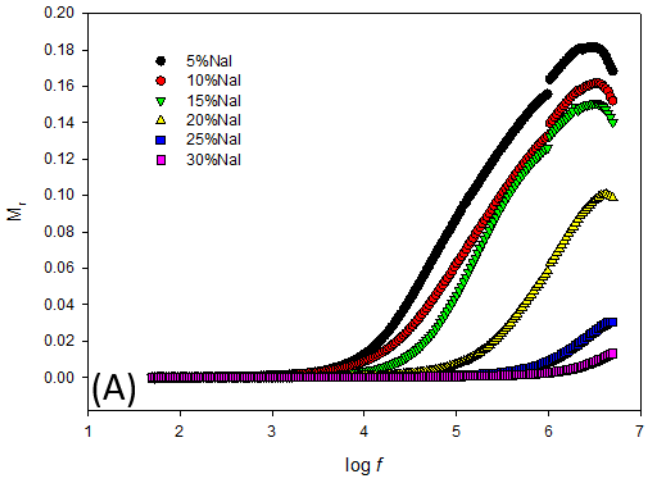

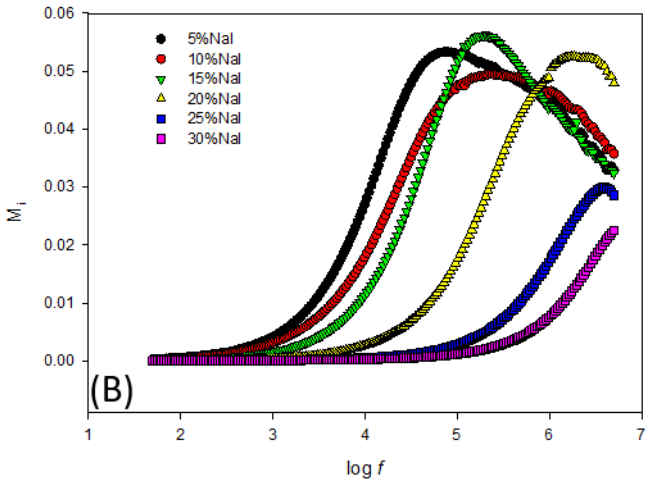

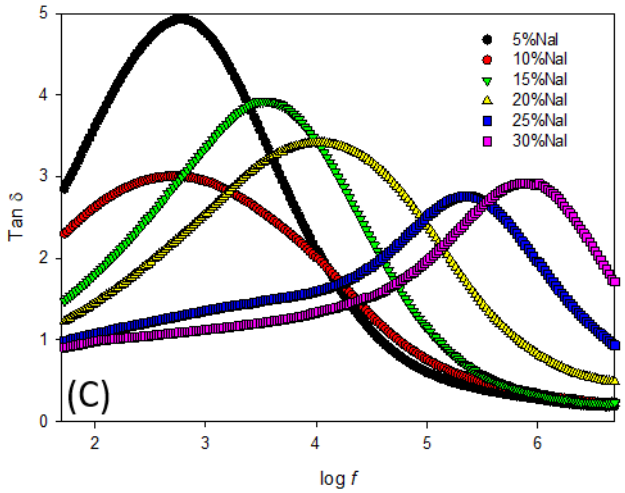

Figure 4. The variation of **(a)** M_r and **(b)** M_i *vs.* frequency for biopolymeric SPEs laden with different amounts of NaI salt at room temperature. **(c)** $\tan\delta$ evolution as a function of frequency for biopolymeric SPEs laden with different amounts of NaI; data refer to room temperature.

$\tan\delta$ is the ratio of energy loss to energy stored in the electric field, also known dissipation factor. The relaxation behaviour of the polymer electrolyte can be observed through this analysis. The variation of $\tan\delta$ as a function of frequency for biopolymeric SPEs containing different amounts of NaI, measured at room temperature, is show in **Figure 4(c)**. The loss tangent peaks were shifted towards high frequency values as the percentage of NaI increased, passing through the maximum value and then decreasing. This result is consistent with the conductivity values discussed above and indicates that the segmental motion of the sample with NaI 30 wt% is the fastest (shifted to the rightest region), hence requiring only a smallest relaxation time than the others.

Further investigation was carried out as a function of temperature. **Figure 5** depicts the frequency dependence of ε_r and ε_i, respectively, when raising temperature, while **Figure 6** shows the frequency dependence of the real and the imaginary parts of the dielectric modulus, respectively, at different temperatures. ε_r and ε_i values increased with temperature, a condition in which the degree of salt dissociation raised causing an increase of charge carriers density. From **Figure 6**, a long tail is clearly observed at low frequency, which is ascribed to the large capacitance value resulting from electrode polarization. The values of M_r and M_i decrease at high temperature, maybe due to the reduced resistance of the samples. As temperature increases, the graph shifts toward right, *i.e.* towards higher frequencies. This also highlights the increase of electrode polarization in the samples [37]. At low frequency of the imaginary part of dielectric modulus, the temperature peaks can be observed as asymmetrical and broad, showing the distribution of

relaxation times. Nevertheless, these peaks disappeared when the temperature became higher, possibly due to the limitation of frequencies used in this analysis.

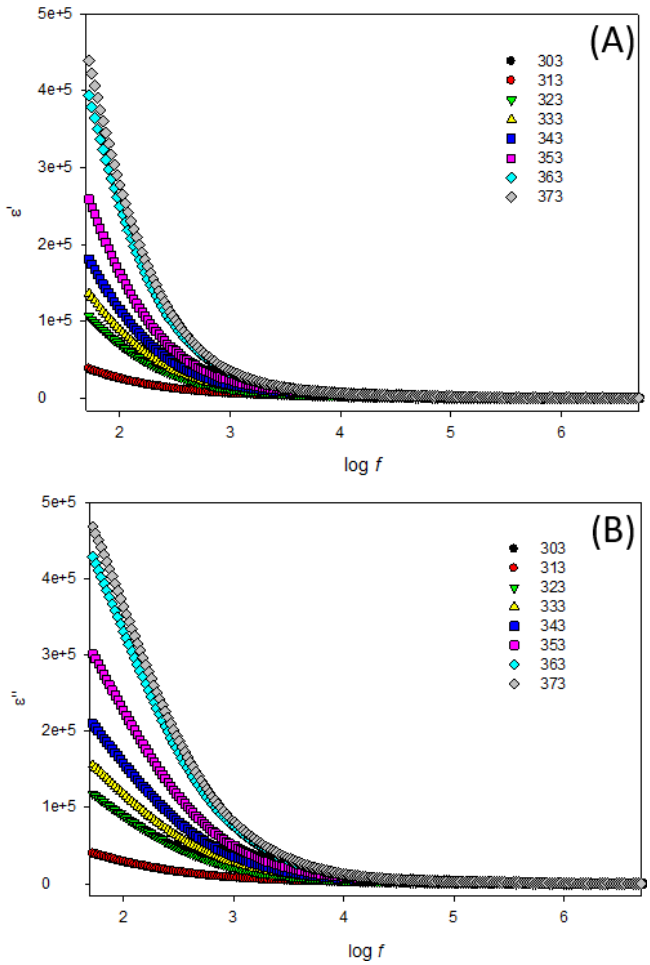

Figure 5. Frequency dependence of **(a)** ε_r and **(b)** ε_i at different temperatures for a biopolymeric SPE containing NaI 30 wt%.

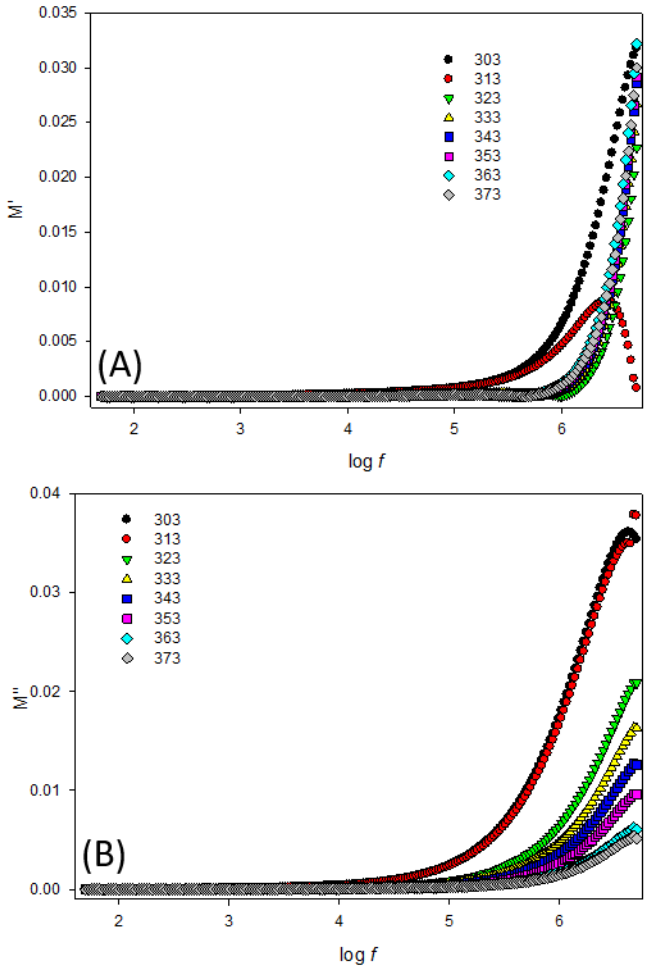

Figure 6. Frequency dependence of **(a)** M_r and **(b)** M_i at different temperatures for a biopolymeric SPE containing NaI 30 wt%.

3.2 Infrared spectroscopy analysis

Through FTIR spectroscopy analysis, the interaction between NaI salt and chitosan matrix was examined by observing the wavenumber shifting of functional groups, such as hydroxyl (O–H), carbonyl (C=O) and amide ($C(O)NH_2$) moieties, when the amount of NaI raised from 5 to 30 wt%, keeping pristine chitosan as a reference. The resulting infrared spectra are shown in **Figure 7** and the main signals are listed in **Table 1**. The peak at 3355 cm^{-1} corresponds to the O–H group, characterized by a strong and broad stretching. This peak is overlapped with a N–H signal at 3285 cm^{-1}. The axial asymmetric and symmetric stretching peaks of C–H are present at 2875 cm^{-1} and 2919 cm^{-1}, respectively. All amide groups of chitosan, which are present at 1646 cm^{-1}, 1561 cm^{-1}

and 1306 cm^{-1}, are linked to the C=O stretching (amide I), N–H bending (amide II) and C–N stretching (amide III), respectively. Symmetric and asymmetric stretching vibrations of C–O and C–O–C polysaccharide skeleton are evident in the range of 1151–895 cm^{-1}. These are all the important peaks for the chitosan control system, which also appeared in a previous work by Rahman *et al.* [71]. It is vital to identify the polar group as well as electronegative atoms in this spectrum, which will provide coordination sites for cations conduction [72,73].

Table 1. Peak of important functional groups in biopolymeric SPEs based on various NaI contents.

Signal type and wavenumber	**Pristine**	**NaI 5 wt%**	**NaI 10 wt%**	**NaI 15 wt%**	**NaI 20 wt%**	**NaI 25 wt%**	**NaI 30 wt%**
O–H	3355	3355	3355	3355	3355	3358	3360
N–H	3287, 3089	3271	3271	3275	3275	3275	3278
C–H (sym)	2875	2877	2877	2877	2879	2883	2885
C–H (asym)	2919						
C=O (amide I)	1652	1634	1634	1634	1634	1632	1633
N–H (amide II)	1561	1543	1543	1543	1543	1543	1547
CH_3 deform	1419, 1377	1407	1407	1405	1409	1407	1409, 1412
CH_2 deform (scissor)	1454	-	-	-	-	-	1462
C–N (amide III)	1320	1378	1378	1378	1378	1378	1404
C–O–C bridge	1153	1150	1150	1150	1150	1150	1150
N–H bend	898	900	900	900	-	900	901
C–O stretch	1026, 1060	-	-	-	-	-	1018, 1065

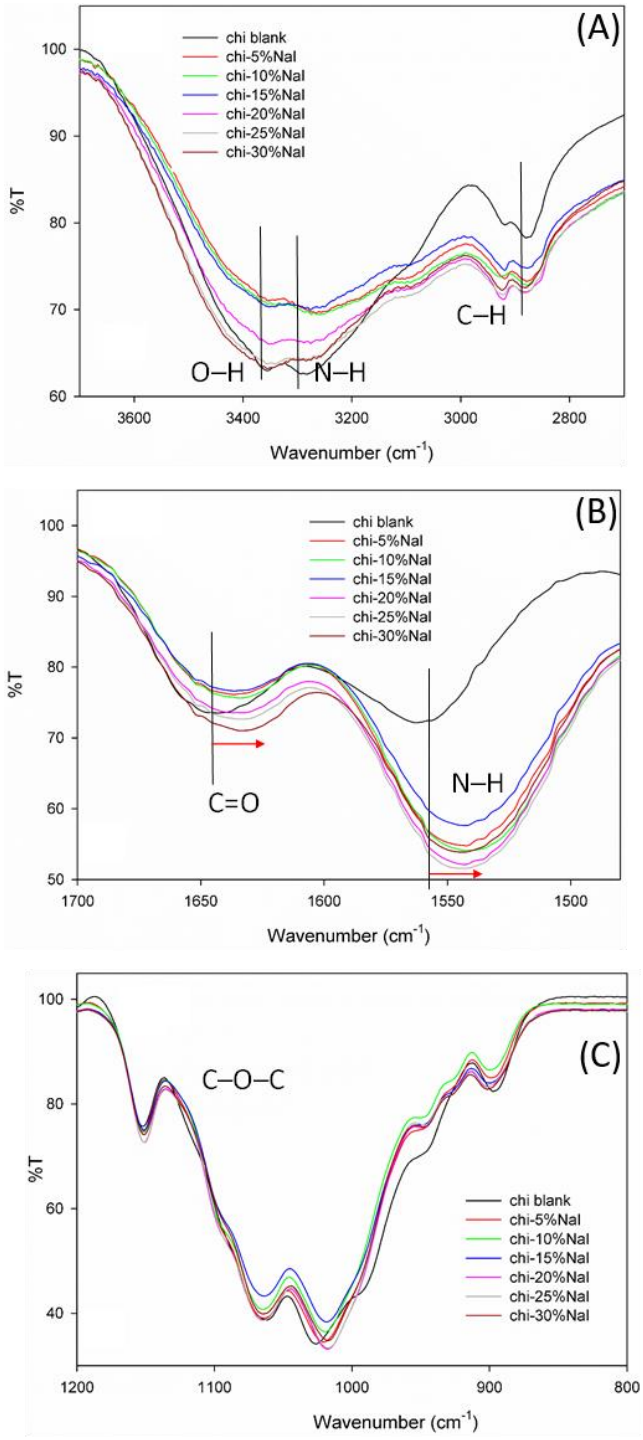

Figure 7. FTIR spectra of **(a)** hydroxyl, **(b)** carbonyl (amide I), N–H (amide II) and **(c)** ether group of biopolymeric SPEs based on various NaI contents.

From **Figure 7(a)**, the hydroxyl band at 3355 cm^{-1} becomes broader when NaI content increases in the electrolyte composition. These changes highlight the existence of interactions between chitosan matrix and ions coming from salt dissociation, *i.e.* a polymer-salt complexes form. The

amide I band, which is also known as carboxamide (O=C–NHR), slightly shifted to 1631 cm^{-1}, whereas the amide II band shifted to 1544 cm^{-1}, as shown in **Figure 7(b)**. Besides that, the C–O stretching peak at 1026 cm^{-1} shifted to 1017 cm^{-1}; this peak is typically named C–H rocking [74]. Another shift is seen for C–N (amide III), from 1317 cm^{-1} to 1320 cm^{-1}. This peak can also be assigned as C–O group in polysaccharide and also as C–H [75]. Another shift was that of N–H bending from 895 cm^{-1} to 901 cm^{-1}, which also represents the C1 group of the β-glycosidic linkage [76].Conversely, the ether signal (asymmetric stretching C–O–C) at 1152 cm^{-1} does not show any significant shift. From these FTIR results, it can be concluded that complexation took place between salt and chitosan. In particular, interactions formed between the oxygen in the carbonyl group of chitosan and Na^+ from the salt, and also between the carbon of the carbonyl group and the I^- from the salt. Na^+ is a positive ion, so it interacts with electron rich atoms, like oxygen of carbonyl group in the chitosan chain and nitrogen from the amide group, while iodide anion seeks an electron-deficient atom, like the carbonyl carbon. These two interactions lead to an overall shift of the C=O stretching. The shifting phenomena can be of two types: i) shifting to higher wavenumbers, due to the strong stretching and shorter bond; ii) shifting to lower wavenumbers, due to the weak stretching that makes the bond longer between the atoms in the functional group, as shown in **Scheme 1**. The unchanged peak of ether is because the coordination of Na^+ ion is preferential to carbonyl due to the higher electron density of oxygen atom of carbonyl compared to the ether. The result is significant to prove the occurrence of complexation between the polymer host and the added salt when all of the wavenumbers were shifted more than 2 cm^{-1}, as reported by Dzulkarnain *et al.* [77].This result can also be supported by XRD diffractograms (shown in the next section), which show that the increment of NaI salt led to a crystallinity reduction of the electrolyte sample, which results in the optimum conductivity determined for the electrolyte laden with NaI 30 wt%. **Scheme 1** summarizes the possible interaction mechanisms of chitosan with NaI

in the biopolymeric SPE system. A strong interaction between the polar functional groups of ether, hydroxyl and carbonyl moieties with sodium ions takes place, as clearly proved by FTIR spectra.

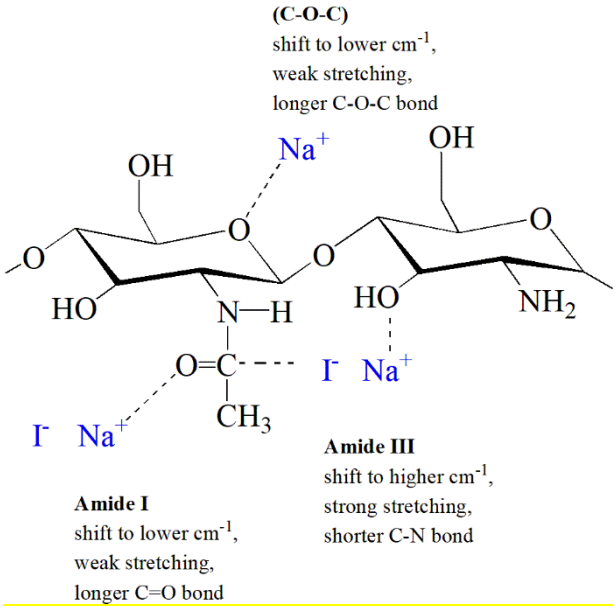

Scheme 1. Mechanism of stretching in chitosan when NaI salt is added.

2.3 Structural analysis

Crystallinity nature and pattern in biopolymeric SPEs were analysed by XRD method. The patterns of pure NaI salt and biopolymeric SPEs laden with NaI 5-30 wt% are shown in **Figure 8**. Sharp and intense peaks are observed at 2θ = 21.2°, 23.8°, 32.0°, 32.9°, 40.5° and 49.9° for NaI salt, indicating that the salt possesses high crystallinity. From the diffractogram of the chitosan control system, it can be seen that several broad humps with small peaks appear at 2θ = 12.8º and 20.6º, which are also known as crystal forms I and II, respectively [78].These patterns represent the crystallinity properties for a pure chitosan film. The XRD pattern of the biopolymeric SPE at 2θ = 12.8º and 20.6º gradually decreased with the increase of NaI salt concentration. Also, the peak corresponding to pure NaI disappeared from the spectrum of the biopolymeric SPEs, which revealed the complete dissolution of the salt in the chitosan host matrix. The disruption of the intramolecular interactions between Na^+ and functional groups in chitosan chains reduced the

crystallinity of the biopolymeric SPE, thus the absence of peaks with the addition of salt indicated that complexation occurred between salt and host matrix. As regards the pristine biopolymer, the crystalline peaks result from the strong intermolecular interaction between polymer chains through the intermolecular hydrogen bonding [79].The three humps in the chitosan-based SPE started to be reduced and disrupted, thus the intensity of crystallinity peaks decreased drastically upon addition of salt [80]. It can be seen that the sample with NaI 30 wt% shows the lowest crystallinity. It is well known that reduction of crystallinity of the polymer enhances its amorphous domains [39], this latter conferring higher conductivity to the biopolymeric SPE [81]. Thus, its mobile ions will move easier between cell electrodes, taking advantage of the enlarged amorphous domains with respect to the crystalline counterparts. As a result, greater ionic conductivity can be obtained [82]. Therefore, the sample with the optimal conductivity was demonstrated to be the one possessing the lowest crystallinity degree in our study. This result can also be supported by FTIR spectra (shown in the previous section), which highlighted the significant shifting caused by the dissociation of salt and interaction with the biopolymeric host, making it more amorphous.

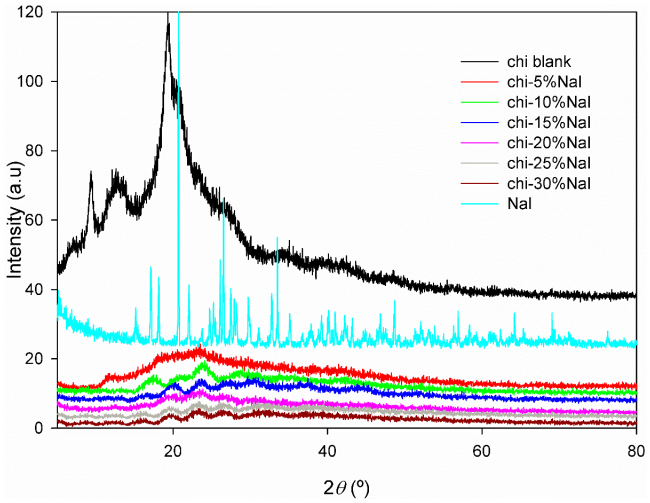

Figure 8. XRD pattern of biopolymeric SPEs containing different amounts of NaI.

3.4 Morphological analysis

Changes in morphology of chitosan upon NaI addition were determined by SEM. Micrographs of pristine chitosan are shown in **Figure 9(a)**, while **Figure 9(b-d)** shows images of biopolymeric SPEs taken at ×500 and ×10000 magnification degrees. The chitosan reference sample showed a rough surface morphology, much more with respect to the SPE. This was compatible with the wide crystalline domains detected by XRD analysis for pristine chitosan; as a consequence, a loose and uneven surface with many small crater-valley type structures was clearly observed. With the addition of NaI, the sample surface becomes smoother. This might be due to the increased concentration of ions, that move more freely at the electrode/electrolyte interface if the electrolyte possesses a smoother surface [36,49], leading to the detected enhancement in ionic conductivity, as already demonstrated in the literature [72]. Furthermore, the smooth surface morphology indicated that salt was completely dissolved in the polymeric matrix, thus certifying the existence of interaction between salt and polymer host. Besides that, no phase separation between the biopolymer and the salt crystals was observed in all NaI/chitosan samples [63]. The results coming from SEM, FTIR and XRD characterizations were in good agreement with the conductivity measurements, where the sample with highest ionic conductivity showed significant salt-polymer interactions and a lowering of crystalline domains.

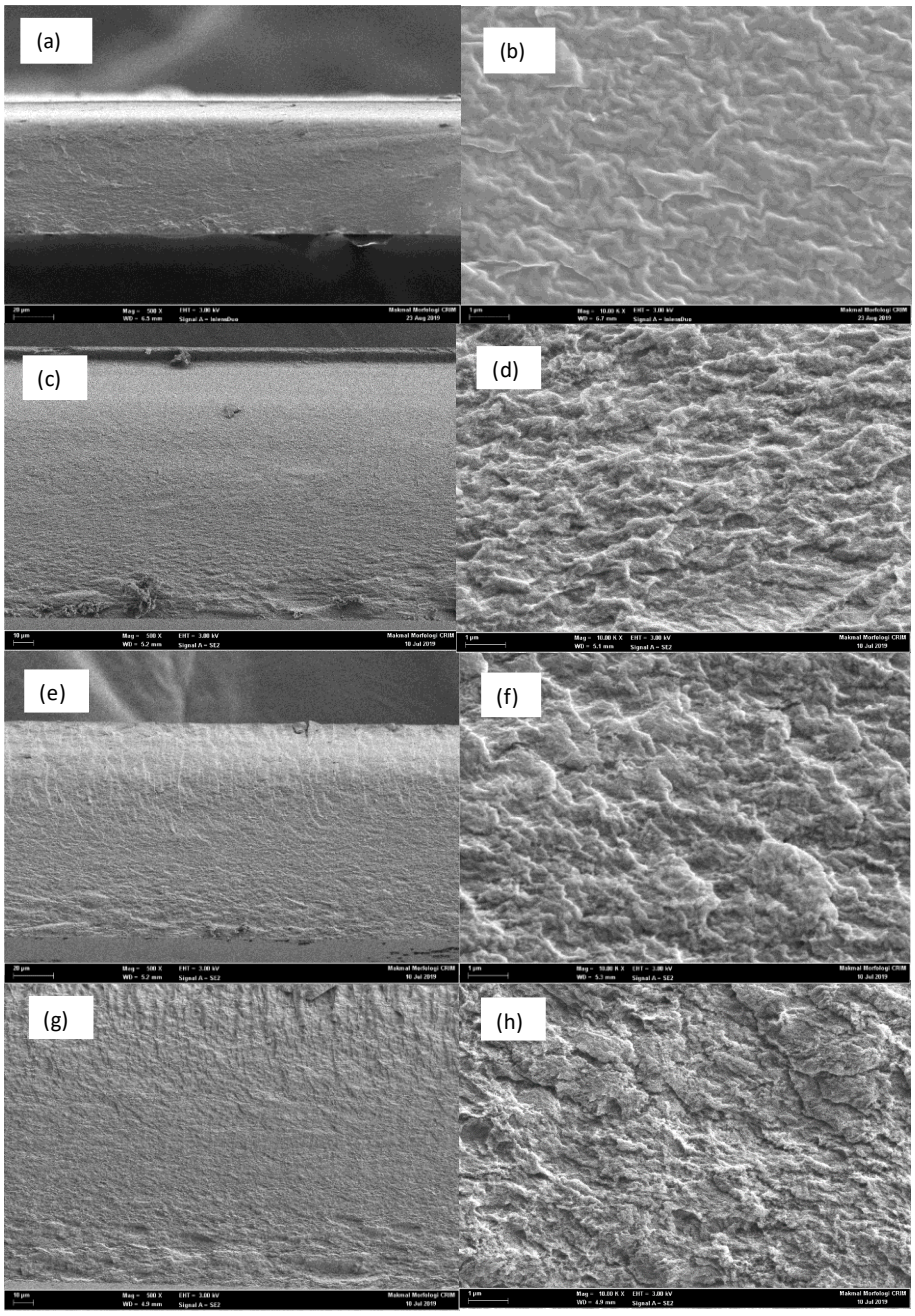

Figure 9. SEM micrographs at ×500 and ×10000 magnification degrees for **(a,b)** pure chitosan and biopolymeric SPEs laden with **(c,d)** NaI 10 wt%, **(e,f)** NaI 20 wt% and **(g,h)** NaI 30 wt%.

3.5 Thermal analysis

Thermal stability of biopolymeric SPEs was determined by TGA. The resulting data are shown in **Table 2**, while the thermograms are given in **Figure 10(a,b)**. It emerges that pristine chitosan possesses two weight loss steps. The first loss was equal to 12.36%, peaking at 41.88 °C, mainly

attributed to water coming from moisture absorption from surroundings and residuals from the acetic acid solution used to process the biopolymer. The second weight loss started at 259 °C and ended at 287 °C; it was attributed to the thermal degradation of chitosan matrix [83].As regards biopolymeric SPEs, two weight loss steps were again observed and attributed to the same phenomena described above. Overall, the sample laden with NaI 30 wt% showed good thermal stability, being its main weight loss starting at 260 °C. This demonstrates that it possesses appreciable thermal properties, that are suitable for electrochemical devices applications.

Table 2 Thermal data for pristine chitosan and biopolymeric SPEs.

Sample	**Weight loss (wt%)**		**Residual mass (wt%)**	**Maximum degradation temperature (T_{max} (°C))**	**Glass transition temperature (T_g)**
	Temperature range (50-170 °C)	**Temperature range (170-600 °C)**			
Chitosan	13	44	43	278	87
+ NaI 10 wt%	15	42	43	270	N.A.
+ NaI 20 wt%	13	39	48	267	N.A.
+ NaI 30 wt%	13	45	42	278	81

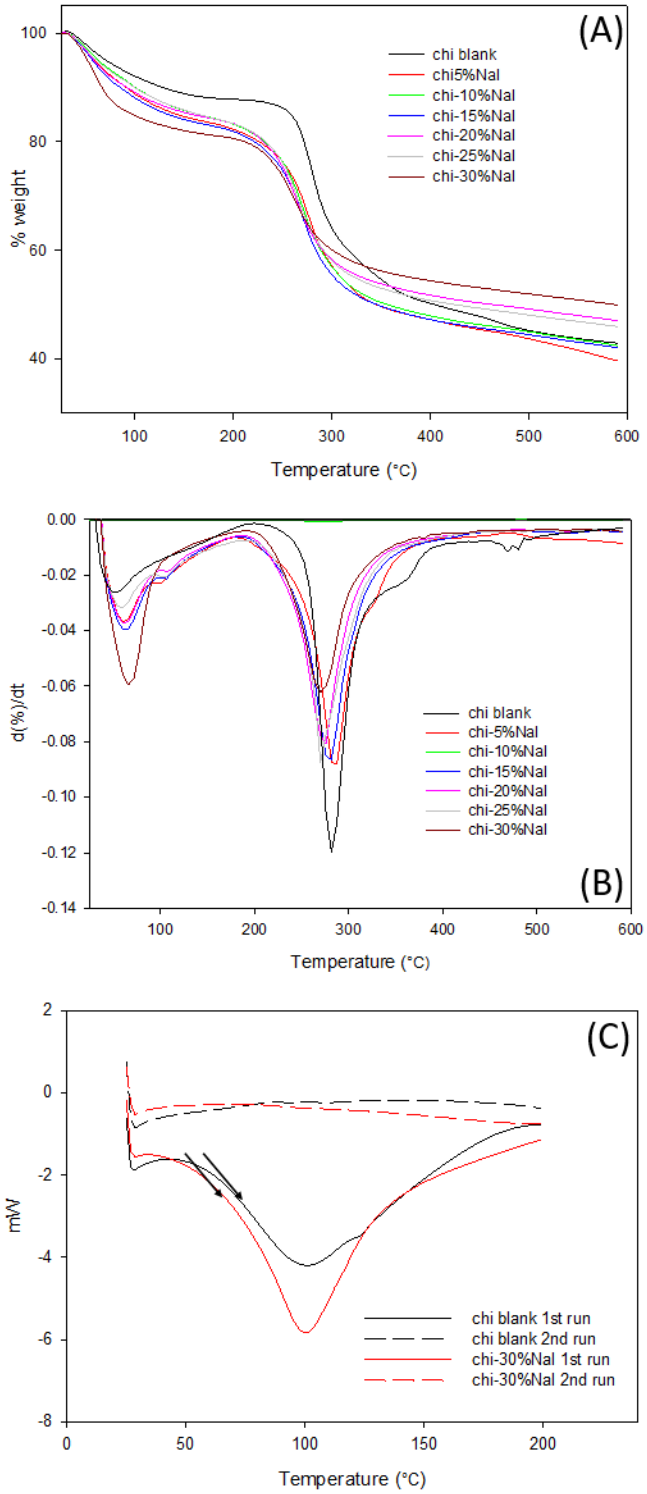

Figure 10. (a) TGA and **(b)** its derivative for pristine chitosan and biopolymeric SPEs. **(c)** DSC thermograms for pristine chitosan and a biopolymeric SPE laden with NaI 30 wt%.

DSC studies were carried out to measure the amount of heat absorbed or released by samples during heating and cooling steps, providing quantitative and qualitative data on endothermic (heat

absorption) and exothermic (heat evolution) processes. From the first DSC run, a peak emerged at 80-100 °C and was attributed to water [71,84]. The second DSC run was carried out to work on moisture-free samples to detect any T_g. However, this signal was not clearly observed (see **Figure 10(c)**). Others works present in the literature found different values of T_g for chitosan matrices [85,86]. For example, El-Hefian *et al.* reported that a T_g for chitosan equal to 140 °C [84]. Anyway, by this measurement we are sure that no transition phenomena occur when our biopolymeric SPE is placed in a DSSC.

3.6 Chronoamperometry analysis

To verify the ionic species activity in the biopolymeric SPEs, transference number measurements were performed. Through this analysis, the correlation between the diffusion phenomena and the conductivity behaviour of the electrolyte can be associated. The normalized current *vs.* time for the biopolymeric SPE containing NaI 30 wt% is plotted in **Figure 11(a)**. It shows that the total ionic transference number for this system is 0.99, calculated through equation (10). This proposes that the charge transport in the biopolymeric SPE is predominantly due to ions (and not electrons). Previous studies by Whba *et al.* proved that the values of t_{ion} increased as ionic conductivity improved [87]. During the transference number measurements, the symmetrical cell polarizes when the ions in the polymer electrolyte film travel to the electrode connected to the terminal that has an opposite charge to that of their own. Any residual current flow passes through the migration of electron across the electrolyte and interfaces. The initial total current decreases and it can be monitored over time (after several hours), due to the depletion of the ionic species in the electrolyte, until it becomes constant in the fully depleted state. If the electrolyte conduction mechanism is primarily ionic, the ionic currents go through an ion-blocking electrode and fall rapidly with time. In the biopolymeric SPE, the ionic species involved are cations and anions. The possible ionic mobility in this system is attributed to Na^+, H^+, CH_3COO^- and I^-. In order to substantiate which

ionic species dominate in this chitosan-based electrolyte, t_{Na^+} analysis was carried out accordingly to equation (12) [46].

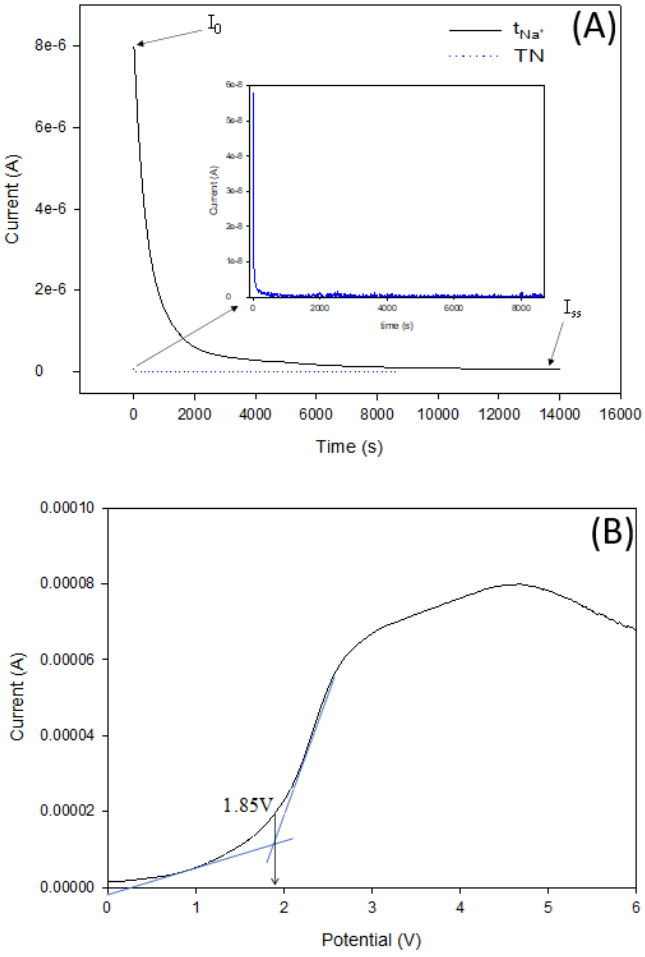

Figure 11. (a) Chronoamperogram of total ion transference number and total sodium ion transport of a biopolymeric SPE containing NaI 30 wt%. **(b)** Linear sweep voltammetry curve for the chitosan-30 wt% NaI.

Total number of sodium ion charges contribution was calculated by Equation (12). t_{Na^+} value was 0.009 (*i.e.*, 0.9%). This suggested that the charge transport in the biopolymeric SPE was predominantly due to iodide ions, which approximately take care of 99.1% of the whole ions transport. During the measurement of t_{Na^+}, the mechanism of ions is the same as total ion measurement.

3.7 Voltammetry analysis

The potential range where polymer electrolytes can work is important and needs to be evaluated before they are used in any electrochemical device, such as batteries, solar cells and other energy conversion/storage systems. LSV plot, shown in **Figure 11(b)**, represents the current-voltage response of our biopolymeric SPE. It shows that the decomposition potential voltage for samples containing NaI 30 wt% is 1.85 V, as evidenced from the tangent intercept with the *x*-axis. This result highlights that the biopolymer SPE proposed in this work is very suitable and perfectly fits with DSSCs applications, the working potential of which are usually below 1 V. It is also suitable for proton batteries, because the electrochemical window of these devices is around 1 V [35,88].

3.8 Solar cells performance

Photovoltaic performance were evaluated through I-V measurements, carried out on different cell configurations: i) FTO/TiO_2-N719/Biopolymeric_SPE_I_2/Pt, ii) FTO/TiO_2-N719/Iodolyte_LE/Pt and iii) FTO/TiO_2-N719/NaI_I_2_LE/Pt. The photovoltaic parameters were obtained from the intersection of current and voltage axes with the I–V curve and further elaboration, as detailed in equations (13) and (14). **Figure 12(a)** plots the photocurrent density-voltage (J–V) curves for DSSCs assembled with the biopolymeric SPE, the commercial Iodolyte LE and a home-made LE consisting of NaI/I_2. The cell with the biopolymeric SPE showed a photovoltaic response characterized by J_{sc} of 0.3 mA cm^{-2}, V_{oc} of 0.7 V, FF of 0.30 and η of 0.06%; these data were consistent in five replicas. Therefore, this proved that the newly proposed SPE has the potential to be applied in DSSCs. The performance of the liquid-state devices was obviously better, but they are subjected to organic solvent evaporation upon time; after one month, the solid-state devices perfectly kept their initial efficiency, while LE-based cells lost 85% of their starting performance.

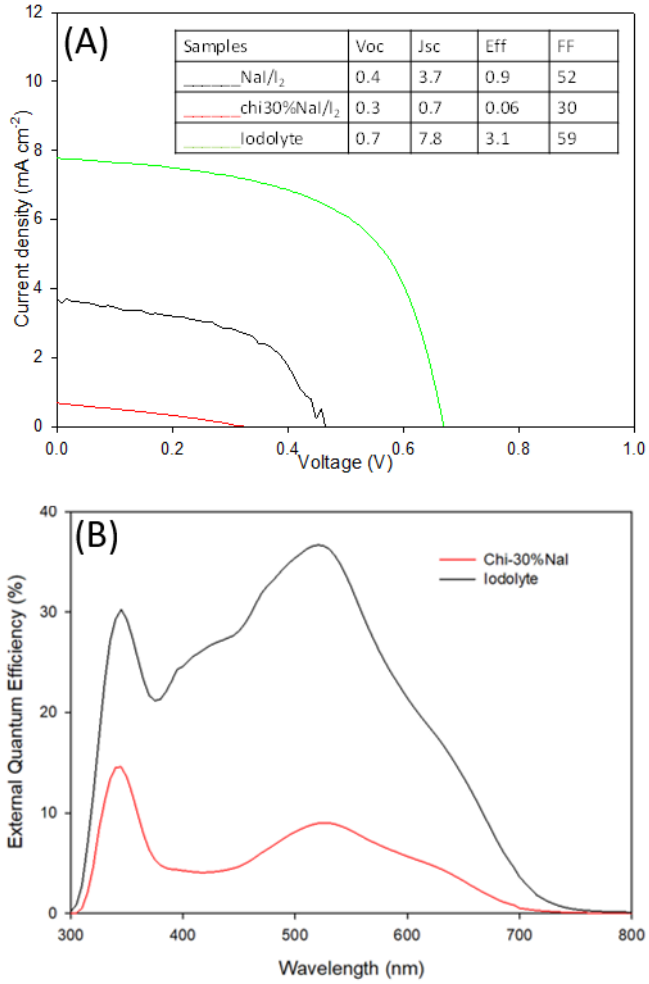

Figure 12. (a) J–V and **(b)** IPCE curves of DSSCs assembled with different electrolytes.

IPCE is the ratio describing how many electrons are generated by a solar cell in function of the incident photons, impimping on the device, calculated by equations (15) and (16). It is well-known that IPCE is determined by three factors, *i.e.* the light harvesting of dye, the efficiency of electron injection and the collection efficiency of the injected electron. **Figure 12(b)** shows the IPCE spectra of DSSCs assembled with the three configurations described in the previous section. Two absorption maximum peaks appeared at 348 nm and 516 nm, typical of N719-sensitized solar cells [89,90]. Cells containing the Iodolyte electrolyte showed a maximum IPCE of 36%, while devices fabricated with the biopolymeric SPE achieved a IPCE close to 9%. These results may be due to

the slower ions transfer mechanism in the SPE, which is known to be slower than the liquid counterpart, as well as to the worse interface at the photoanode/electrolyte side [91].

4. Conclusions

Chitosan-based SPEs incorporating with various percentages of NaI were successfully prepared by a solution casting method. From FTIR studies, the complexation between NaI and chitosan was confirmed by the shift of hydroxyl, amine and carboxamide bands of the biopolymeric matrix. From the XRD results, the electrolyte was found to be less crystalline in comparison to the pristine chitosan matrix. The best ionic conductivity obtained was 1.11×10^{-4} S cm^{-1} with NaI 30 wt%, where the contribution from ions motion was 99%. The Na^+ transference number analysis indicated ionic mobile species were predominantly iodine anions of the redox couple mediator in this system, which is truly suitable for DSSC application. The best biopolymeric SPE sample showed a J_{sc} of 0.3 mA cm^{-2}, a V_{oc} of 0.7 V, a *FF* of 0.30 and a η of 0.06% when used in lab-scale DSSCs. The current study paves the way to the use of biopolymeric matrices for 100% solid-state DSSCs.

Acknowledgments

The authors would like to thank Universiti Kebangsaan Malaysia (UKM) for financial support through the grant code FRGS/1/2016/TK07/UKM/02/2. Special thanks to the Faculty of Science and Technology (FST), Solar Energy Research Institute (SERI) and Centre for Research and Instrumentation Management (CRIM) at UKM for providing technical and facilities. Politecnico di Torino is gratefully acknowledged by F.B. for granting the fund named “Contributo ERC per chi ha superato il primo step di valutazione”.

References

[1] S. Impram, S. Varbak Nese, B. Oral, Challenges of renewable energy penetration on power system flexibility: a survey, Energy Strateg. Rev. 31 (2020) art. no. 100539.

[2] G.E. Halkos, E.C. Gkampoura, Reviewing usage, potentials, and limitations of renewable energy sources, Energies 13 (2020) art. no. 2906.

[3] G.W. Huang, C.T. Li, Y.C. Chen, R.J. Jeng, S.A. Dai, Synthesis and properties of polyurea/malonamide dendritic co-adsorbents for dye-sensitized solar cells, Polymer 179 (2019) art. no. 121673.

[4] N.K. Farhana, S. Bashir, S. Ramesh, K. Ramesh, Augmentation of dye-sensitized solar cell photovoltaic conversion efficiency via incorporation of terpolymer Poly(vinyl butyral-co-vinyl alcohol-co-vinyl acetate) based gel polymer electrolytes, Polymer 223 (2021) art. no. 123713.

[5] N. Sangiorgi, A. Sanson, Influence of electropolymerized polypyrrole optical properties on bifacial dye-sensitized solar cells, Polymer 125 (2017) 208-216.

[6] S.K. Tseng, R.H. Wang, J.L. Wu, J.P. Jyothibasu, T.L. Wang, C.Y. Chu, R.H. Lee, Synthesis of a series of novel imidazolium-containing ionic liquid copolymers for dye-sensitized solar cells, Polymer 210 (2020) art. no. 123074.

[7] M.A.M. Al-Alwani, A.B. Mohamad, N.A. Ludin, A.A.H. Kadhum, K. Sopian, Dye-sensitised solar cells: development, structure, operation principles, electron kinetics, characterisation, synthesis materials and natural photosensitisers, Renewable Sustainable Energy Rev. 65 (2016) 183-213.

[8] F. Bella, A. Lamberti, S. Bianco, E. Tresso, C. Gerbaldi, C.F. Pirri, Floating, flexible polymeric dye-sensitized solar-cell architecture: the way of near-future photovoltaics, Adv. Mater. Technol. 1 (2016) art. no. 1600002.

[9] S. Mathew, A. Yella, P. Gao, R. Humphry-Baker, B.F.E. Curchod, N. Ashari-Astani, I. Tavernelli, U. Rothlisberger, M.K. Nazeeruddin, M. Grätzel, Dye-sensitized solar cells with 13% efficiency achieved through the molecular engineering of porphyrin sensitizers, Nat. Chem. 6 (2014) 242-247.

[10] A. Yella, H.W. Lee, N.H. Tsao, C. Yi, A.K. Chandiran, M.K. Nazeeruddin, E.W.G. Diau, C.Y. Yeh, S.M. Zakeeruddin, M. Grätzel, Porphyrin-sensitized solar cells with cobalt (II/III)-based redox electrolyte exceed 12 percent efficiency, Science 334 (2011) 629-634.

[11] D.A. Chalkias, D.D. Loizos, G.C. Papanicolaou, Evaluation and prediction of dye-sensitized solar cells stability under different accelerated ageing conditions, Sol. Energy 207 (2020) 841-850.

[12] P. Manafi, H. Nazockdast, M. Karimi, M. Sadighi, L. Magagnin, A study on the microstructural development of gel polymer electrolytes and different imidazolium-based ionic liquids for dye-sensitized solar cells, J. Power Sources 481 (2021) art. no. 228622.

[13] K.K.M. Masud, H.K. Kim, Polymer gel electrolytes based on PEG-functionalized ABA triblock copolymers for quasi-solid-state dye-sensitized solar cells: molecular engineering and key factors, ACS Appl. Mater. Interfaces 12 (2020) 42067-42080.

[14] D.E. Fenton, J.M. Parker, P.V. Wright, Complexes of alkali metal ions with poly(ethylene oxide), Polymer 14 (1973) 589.

[15] H. Wang, L. Sheng, G. Yasin, L. Wang, H. Xu, X. He, Reviewing the current status and development of polymer electrolytes for solid-state lithium batteries, Energy Storage Mater. 33 (2020) 188-215.

[16] J. Mindemark, M.J. Lacey, T. Bowden, D. Brandell, Beyond PEO - alternative host materials for Li^+-conducting solid polymer electrolytes, Prog. Polym. Sci. 81 (2018) 114-143.

[17] X. Yang, M. Jiang, X. Gao, D. Bao, Q. Sun, N. Holmes, H. Duan, S. Mukherjee, K. Adair, C. Zhao, J. Liang, W. Li, J. Li, Y. Liu, H. Huang, L. Zhang, S. Lu, Q. Lu, R. Li, C.V. Singh, X. Sun, Determining the limiting factor of the electrochemical stability window for PEO-based solid polymer electrolytes: main chain or terminal -OH group?, Energy Environ. Sci. 13 (2020) 1318-1325.

[18] S. Chen, F. Feng, H. Che, Y. Yin, Z.F. Ma, High performance solid-state sodium batteries enabled by boron contained 3D composite polymer electrolyte, Chem. Eng. J. 406 (2021) art. no. 126736.

[19] S.S. Gaur, P. Dhar, A. Sonowal, A. Sharma, A. Kumar, V. Katiyar, Thermo-mechanically stable sustainable polymer based solid electrolyte membranes for direct methanol fuel cell applications, J. Membr. Sci. 526 (2017) 348-354.

[20] M. Raja, B. Sadhasivam, R. Janraj Naik, R. Dhamodharan, K. Ramanujam, A chitosan/poly(ethylene glycol)-ran-poly(propylene glycol) blend as an eco-benign separator and binder for quasi-solid-state supercapacitor applications, Sustainable Energy Fuels 3 (2019) 760-773.

[21] C.W. Kuo, W.B. Li, P.R. Chen, J.W. Liao, C.G. Tseng, T.Y. Wu, Effect of plasticizer and lithium salt concentration in PMMA-based composite polymer electrolytes, Int. J. Electrochem. Sci. 8 (2013) 5007-5021.

[22] S. Ramesh, C.W. Liew, E. Morris, R. Durairaj, Effect of PVC on ionic conductivity, crystallographic structural, morphological and thermal characterizations in PMMA-PVC blend-based polymer electrolytes, Thermochim. Acta 511 (2010) 140-146.

[23] T. Winie, N.S. Mohd Shahril, Conductivity enhancement by controlled percolation of inorganic salt in multiphase hexanoyl chitosan/polystyrene polymer blends, Front. Mater. Sci. 9 (2015) 132-140.

[24] J.K Park, Principles and Applications of Lithium Secondary Batteries, Wiley, Weinheim, 2012.

[25] J.E. Nair, C. Gerbaldi, M. Destro, R. Bongiovanni, N. Penazzi, Methacrylic-based solid polymer electrolyte membranes for lithium-based batteries by a rapid UV-curing process, React. Funct. Polym. 71 (2011) 409-416.

[26] W. Wang, X. Guo, Y. Yang, Lithium iodide effect on the electrochemical behavior of agarose based polymer electrolyte for dye-sensitized solar cell, Electrochim. Acta 56 (2011) 7347-7351.

[27] M. Kumar, T. Tiwari, N. Srivastava, Electrical transport behaviour of bio-polymer electrolyte system: Potato starch + ammonium iodide, Carbohydr. Polym. 88 (2012) 54-60.

[28] S.D. Pasini Cabello, S. Mollá, N.A. Ochoa, J. Marchese, E. Giménez, V. Compañ, New bio-polymeric membranes composed of alginate-carrageenan to be applied as polymer electrolyte membranes for DMFC, J. Power Sources 265 (2014) 345-355.

[29] N.N. Mobarak, N. Ramli, M.P. Abdullah, A. Ahmad, Spectroscopic studies of carboxymethyl chitosan-ammonium triflate ($NH_4CF_3SO_3$) based solid polymer electrolytes, AIP Conf. Proc. 1571 (2013) 843-849.

[30] A.S.A. Khiar, R. Puteh, A.K. Arof, Conductivity studies of a chitosan-based polymer electrolyte, Physica B 373 (2006) 23-27.

[31] E. Raphael, C.O. Avellaneda, M.A. Aegerter, M.M. Silva, A. Pawlicka, Agar-based gel electrolyte for electrochromic device application, Mol. Cryst. Liq. Cryst. 554 (2012) 264-272.

[32] R. Rahamathullah, W.M. Khairul, M.I.N. Isa, Contribution of stilbene-imine additives on the structural, ionic conductivity performance and theoretical evaluation on CMC-based biopolymer electrolytes, Carbohydr. Polym. 250 (2020) art. no. 116935.

[33] M. Rinaudo, Chitin and chitosan: Properties and applications, Prog. Polym. Sci. 31 (2006) 603-632.

[34] M.F.Z. Kadir, S.R. Majid, A.K. Arof, Plasticized chitosan-PVA blend polymer electrolyte based proton battery, Electrochim. Acta 55 (2010) 1475-1482.

[35] L.S. Ng, A.A. Mohamad, Effect of temperature on the performance of proton batteries based on chitosan-NH_4NO_3-EC membrane, J. Membr. Sci. 325 (2008) 653-657.

[36] S.R. Majid, A.K. Arof, Proton-conducting polymer electrolyte films based on chitosan acetate complexed with NH_4NO_3 salt, Physica B 355 (2005) 78-82.

[37] S.B. Aziz, O.G. Abdullah, S. Al-Zangana, Solid polymer electrolytes based on chitosan: NH_4Tf modified by various amounts of TiO_2 filler and its electrical and dielectric characteristics, Int. J. Electrochem. Sci. 14 (2019) 1909-1925.

[38] S.B. Aziz, M.H. Hamsan, W.O. Karim, M.F.Z. Kadir, M.A. Brza, O.G. Abdullah, High proton conducting polymer blend electrolytes based on chitosan: Dextran with constant specific capacitance and energy density, Biomolecules 9 (2019) art. no. 267.

[39] Y.M. Yusof, H.A. Illias, M.F.Z. Kadir, Incorporation of NH_4Br in PVA-chitosan blend-based polymer electrolyte and its effect on the conductivity and other electrical properties, Ionics 20 (2014) 1235-1245.

[40] M.H. Buraidah, A.K. Arof, Characterization of chitosan/PVA blended electrolyte doped with NH_4I, J. Non-Cryst. Solids 357 (2011) 3261-3266.

[41] N.A. Aziz, S.R. Majid, R. Yahya, A.K. Arof, Conductivity, structure, and thermal properties of chitosan-based polymer electrolytes with nanofillers, Polym. Adv. Technol. 22 (2011) 1345-1348.

[42] F. Hassan, H.J. Woo, N.A. Aziz, M.Z. Kufian, S.R. Majid, Synthesis of Al_2TiO_5 and its effect on the properties of chitosan-NH_4SCN polymer electrolytes, Ionics 19 (2013) 483-489.

[43] J.F. Du, Y. Bai, W.Y. Chu, L.J. Qiao, The structure and electric characters of proton-conducting chitosan membranes with various ammonium salts as complexant, J. Polym. Sci., Part B: Polym. Phys. 48 (2010) 880-885.

[44] T. Winie, S.R. Majid, A.S.A. Khiar, A.K. Arof, Ionic conductivity of chitosan membranes and application for electrochemical devices, Polym. Adv. Technol. 17 (2006) 523-527.

[45] Z. Osman, Z.A. Ibrahim, A.K. Arof, Conductivity enhancement due to ion dissociation in plasticized chitosan based polymer electrolytes, Carbohydr. Polym. 44 (2001) 167-173.

[46] M.Z.A. Yahya, A.K. Arof, Studies on lithium acetate doped chitosan conducting polymer system, 38 (2002) 1191-1197.

[47] M.Z.A. Yahya, A.K. Arof, Effect of oleic acid plasticizer on chitosan-lithium acetate solid polymer electrolytes, Eur. Polym. J. 39 (2003) 897-902.

[48] N.S. Mohamed, R.H.Y. Subban, A.K. Arof, Polymer batteries fabricated from lithium complexed acetylated chitosan, J. Power Sources 56 (1995) 153-156.

[49] S.R. Majid, N.H. Idris, M.F. Hassan, T. Winie, A.S.A. Khiar, A.K. Arof, Transport studies on filler-doped chitosan based polymer electrolyte, Ionics 11 (2005) 451-455.

[50] Sudaryanto, E. Yulianti, Patimatuzzohrah, Structure and properties of solid polymer electrolyte based on chitosan and ZrO_2 nanoparticle for lithium ion battery, AIP Conf. Proc. 1710 (2016) art. no. 4941464.

[51] R.H.Y. Subban, A.K. Arof, Sodium iodide added chitosan electrolyte film for polymer batteries, Phys. Scr. 53 (1996) 382-384.

[52] S.B. Aziz, Z.H.Z. Abidin, Role of hard-acid/hard-base interaction on structural and dielectric behavior of solid polymer electrolytes based on chitosan-XCF_3SO_3 ($X = Li^+, Na^+, Ag^+$), J. Polym. 2014 (2014) art. no. 906780.

[53] A.K. Arof, M.H. Buraidah, L.P. Teo, S.R. Majid, R. Yahya, R.M. Taha, Characterizations of chitosan-based polymer electrolyte photovoltaic cells, Int. J. Photoenergy 2010 (2010) art. no. 805836.

[54] M.H. Buraidah, L.P. Teo, C.M. Au Yong, S. Shah, A.K. Arof, Performance of polymer electrolyte based on chitosan blended with poly(ethylene oxide) for plasmonic dye-sensitized solar cell, Opt. Mater. 57 (2016) 202-211.

[55] P.K. Singh, B. Bhattacharya, R.K. Nagarale, K.W. Kim, H.W. Rhee, Synthesis, characterization and application of biopolymer-ionic liquid composite membranes, Synth. Met. 160 (2010) 139-142.

[56] M. Khalili, M. Abedi, H.S. Amoli, S.A. Mozaffari, Comparison of chitosan and chitosan nanoparticles on the performance and charge recombination of water-based gel electrolyte in dye sensitized solar cells, Carbohydr. Polym. 175 (2017) 1-6.

[57] S.N.F. Yusuf, M.F. Aziz, H.C. Hassan, T.M.W.J. Bandara, B.E. Mellander, M.A. Careem, A.K. Arof, Phthaloylchitosan-based gel polymer electrolytes for efficient dye-sensitized solar cells, J. Chem. 2014 (2014) art. no. 783023.

[58] S.N.F. Yusuf, A.D. Azzahari, V. Selvanathan, R. Yahya, M.A. Careem, A.K. Arof, Improvement of N-phthaloylchitosan based gel polymer electrolyte in dye-sensitized solar cells using a binary salt system, Carbohydr. Polym. 157 (2017) 938-944.

[59] F.H. Muhammad, T. Winie, Influence of 1-methyl-3-propylimidazolium iodide ionic liquid on the performance of dye-sensitized solar cell using hexanoyl chitosan/poly(vinyl chloride) based polymer electrolyte, Optik 208 (2020) art. no. 164558.

[60] H.J. Woo, S.R. Majid, A.K. Arof, Dielectric properties and morphology of polymer electrolyte based on poly(ε-caprolactone) and ammonium thiocyanate, Mater. Chem. Phys. 134 (2012) 755-761.

[61] S.A. Hashmi, A. Kumar, K.K. Maurya, S. Chandra, Proton-conducting polymer electrolyte. I. The polyethylene oxide+NH_4ClO_4 system, J. Phys. D: Appl. Phys. 23 (1990) 1307-1314.

[62] P.G. Bruce, C.A. Vincent, Steady state current flow in solid binary electrolyte cells, J. Electroanal. Chem. 225 (1987) 1-17.

[63] S. Mamat, M. Faizzi, M. Sukor Su'ait, N. Ahmad Ludin, K. Sopian, N.A. Dzulkurnain, A. Ahmad, L.K. Shyuan, L.T. Khoon, D. Brandell, An investigation of modified natural rubber-based (MG49) polymer electrolyte in dye-sensitized solar cells, Sains Malaysiana 47 (2018) 2667-2676.

[64] H. Ohno, M. Yoshizawa, T. Mizumo, Electrochemical aspects of ionic liquids, Wiley, Hoboken, 2005.

[65] A.M.M. Ali, M.Z.A. Yahya, H. Bahron, R.H.Y. Subban, Electrochemical studies on polymer electrolytes based on poly(methyl methacrylate)-grafted natural rubber for lithium polymer battery, Ionics 12 (2006) 303-307.

[66] A.S.A. Khiar, A.K. Arof, Conductivity studies of starch-based polymer electrolytes, Ionics 16 (2010) 123-129.

[67] J.B. Gunn, Travelling-wave interaction between the optical modes of a polar lattice and a stream of charge carriers, Phys. Lett. 4 (1963) 194-195.

[68] K. Murayama, Y. Nakamura, A. Shibayama, A. Dohi, T. Ohmi, K. Tro, Planar-type Gunn diode of InP, Jpn. J. Appl. Phys. 13 (1974) 662-666.

[69] S.B. Aziz, S.M. Mamand, The study of dielectric properties and conductivity relaxation of ion conducting chitosan: NaTf based solid electrolyte, Int. J. Electrochem. Sci. 13 (2018) 10274-10288.

[70] S. Ramesh, C.W. Liew, A.K. Arof, Ion conducting corn starch biopolymer electrolytes doped with ionic liquid 1-butyl-3-methylimidazolium hexafluorophosphate, J. Non-Cryst. Solids 357 (2011) 3654-3660.

[71] N.A. Rahman, S.A. Hanifah, N.N. Mobarak, M.S. Su'ait, A. Ahmad, L.K. Shyuan, L.T. Khoon, Synthesis and characterizations of o-nitrochitosan based biopolymer electrolyte for electrochemical devices, PLoS One 14 (2019) art. no. e0212066.

[72] S.A.M. Noor, A. Ahmad, I.A. Talib, M.Y.A. Rahman, Morphology, chemical interaction, and conductivity of a PEO-ENR50 based on solid polymer electrolyte, Ionics 16 (2010) 161-170.

[73] N.N. Mobarak, N. Ramli, A. Ahmad, M.Y.A. Rahman, Chemical interaction and conductivity of carboxymethyl κ-carrageenan based green polymer electrolyte, Solid State Ionics 224 (2012) 51-57.

[74] A. Alemdar, M. Sain, Isolation and characterization of nanofibers from agricultural residues - Wheat straw and soy hulls, Bioresour. Technol. 99 (2008) 1664-1671.

[75] H. Kargarzadeh, R.M. Sheltami, I. Ahmad, I. Abdullah, A. Dufresne, Cellulose nanocrystal: A promising toughening agent for unsaturated polyester nanocomposite, Polymer 56 (2015) 346-357.

[76] M. Le Troedec, D. Sedan, C. Peyratout, J.P. Bonnet, A. Smith, R. Guinebretiere, V. Gloaguen, P. Krausz, Influence of various chemical treatments on the composition and structure of hemp fibres, Composites, Part A 39 (2008) 514-522.

[77] N.A. Dzulkurnain, A. Ahmad, N.S. Mohamed, P(MMA-EMA) random copolymer electrolytes incorporating sodium iodide for potential application in a dye-sensitized solar cell, Polymers 7 (2015) 266-280.

[78] R.J. Samuels, Solid state characterization of the structure of chitosan films, J. Polym. Sci., Part B: Polym. Phys. 19 (1981) 1081-1105.

[79] O.G. Abdullah, S.B. Aziz, M.A. Rasheed, Structural and optical characterization of PVA:$KMnO_4$ based solid polymer electrolyte, Results Phys. 6 (2016) 1103-1108.

[80] M.S. Su'Ait, A. Ahmad, K.H. Badri, N.S. Mohamed, M.Y.A. Rahman, C.L.A. Ricardo, P. Scardi, The potential of polyurethane bio-based solid polymer electrolyte for photoelectrochemical cell application, Int. J. Hydrogen Energy 39 (2014) 3005-3017.

[81] K. Sownthari, S.A. Suthanthiraraj, Synthesis and characterization of an electrolyte system based on a biodegradable polymer, eXPRESS Polym. Lett. 7 (2013) 495-504.

[82] T. Sugumaran, D.S. Silvaraj, N.M. Saidi, N.K. Farhana, S. Ramesh, K. Ramesh, S. Ramesh, The conductivity and dielectric studies of polymer electrolytes based on iota-carrageenan with sodium iodide and 1-butyl-3-methylimidazolium iodide for the dye-sensitized solar cells, Ionics 25 (2019) 763-771.

[83] K. Sakurai, T. Maegawa, T. Takahashi, Glass transition temperature of chitosan and miscibility of chitosan/poly(N-vinyl pyrrolidone) blends, Polymer 41 (2000) 7051-7056.

[84] E.A. El-Hefian, E.S. Elgannoudi, A. Mainal, A.H. Yahaya, Characterization of chitosan in acetic acid: Rheological and thermal studies, Turk. J. Chem. 34 (2010) 47-56.

[85] I. Quijada-Garrido, V. Iglesias-González, J.M. Mazón-Arechederra, J.M. Barrales-Rienda, The role played by the interactions of small molecules with chitosan and their transition temperatures. Glass-forming liquids: 1,2,3-propantriol (glycerol), Carbohydr. Polym. 68 (2007) 173-186.

[86] N.E. Suyatma, L. Tighzert, A. Copinet, V. Coma, Effects of hydrophilic plasticizers on mechanical, thermal, and surface properties of chitosan films, J. Agric. Food. Chem. 53 (2005) 3950-3957.

[87] R.A.G. Whba, L. TianKhoon, M.S. Su'ait, M.Y.A. Rahman, A. Ahmad, Influence of binary lithium salts on 49% poly(methyl methacrylate) grafted natural rubber based solid polymer electrolytes, Arabian J. Chem. 13 (2020) 3351-3361.

[88] R. Pratap, B. Singh, S. Chandra, Polymeric rechargeable solid-state proton battery, J. Power Sources 161 (2006) 702-706.

[89] J. Chang, J. Yang, P. Ma, D. Wu, L. Tian, Z. Gao, K. Jiang, L. Yang, Hierarchical titania mesoporous sphere/graphene composite, synthesis and application as photoanode in dye sensitized solar cells, J. Colloid Interface Sci. 394 (2013) 231-236.

[90] A.M. Ramli, M.Z. Razali, N.A. Ludin, Performance enhancement of dye sensitized solar cell using graphene oxide doped titanium dioxide photoelectrode, Malaysian J. Anal. Sci. 21 (2017) 928-940.

[91] M.Y.A. Rahman, M.M. Salleh, I.A. Talib, M. Yahaya, Effect of ionic conductivity of a PVC-$LiClO_4$ based solid polymeric electrolyte on the performance of solar cells of ITO/TiO_2/PVC-$LiClO_4$/graphite, J. Power Sources 133 (2004) 293-297.